Spiral Growth without Dislocations: Molecular Beam Epitaxy of the Topological Insulator Bi_{2}Se_{3} on Epitaxial Graphene/SiC(0001)

Y. Liu, M. Weinert, and L. Li

Phys. Rev. Lett. **108**, 115501 — Published 14 March 2012

DOI: 10.1103/PhysRevLett.108.115501

Spiral growth without dislocations: Molecular beam epitaxy of the topological insulator Bi_2Se_3 on epitaxial graphene/SiC(0001)

Y. Liu, M. Weinert, and L. Li*

Department of Physics

University of Wisconsin, Milwaukee, WI 53211

Abstract:

We report a new mechanism that does not require the formation of interfacial dislocations to mediate spiral growth during molecular beam epitaxy of Bi_2Se_3. Based on *in situ* scanning tunneling microscopy observations, we find that Bi_2Se_3 growth on epitaxial graphene/SiC(0001) initiates with two-dimensional (2D) nucleation, and that the spiral growth ensues with the pinning of the 2D growth fronts at jagged steps of the substrate or at domain boundaries created during the coalescence of the 2D islands. Winding of the as-created growth fronts around these pinning centers leads to spirals. The mechanism can be broadly applied to the growth of other van der Waals materials on weakly interacting substrates. We further confirm, using scanning tunneling spectroscopy, that the one-dimensional helical mode of a line defect is not supported in strong topological insulators such as Bi_2Se_3.

PACS: 81.10.-h, 72.10.Fk, 68.37.Ef, 73.20.-r

*lianli@uwm.edu

Rhombohedral Bi_2X_3 (X=Se, Te) exhibits a layered structure along the [111] direction, where five atomic layers in the sequence of -X-Bi-X-Bi-X- form a quintuple layer (QL) unit with X surface termination [1]. A distinct feature of these alloys is that, despite covalent Bi-X bonding within the QL units, the adjacent QLs are only weakly bonded by van der Waals forces. These alloys have been extensively studied for their thermal electrical applications [2,3], but recently have also generated renewed interests as three-dimensional (3D) topological insulators (TIs) [4], due to theoretical predictions of exotic properties associated with topologically protected helical two-dimensional (2D) surface states [1] and one-dimensional (1D) states associated with bulk line defects such as dislocations [5-7]. While the 2D surface states have been experimentally verified using angle resolved photoelectron spectroscopy [8-10] and scanning tunneling spectroscopy (STS) [11-15], the bulk 1D modes, which also depend on the type of the dislocations (e.g., screw or edge) and the class of the TIs (i.e., strong or weak) [5-7], are yet to be verified experimentally.

Recent studies of Bi_2X_3 alloys have shown the formation of spirals on a variety of substrates such as GaAs(111)B and Si(111) during molecular beam epitaxy (MBE) [16-18]. This is an interesting observation because spirals are commonly thought to originate from misfit dislocations at the interface during hetroepitaxial growth [19-23]. When the dislocations have a screw component, they can emerge at the surface to create additional steps to facilitate the growth of spirals [19-23]. However, in the case of Bi_2X_3 where the adjacent QLs are only weakly bonded by van der Waals forces, the epilayer is not expected to strongly bond to any substrate, i.e., no formation of dislocations to seed the spiral growth. Since MBE offers the possibility to control the synthesis of TIs at the atomic scale, understanding this new spiral growth is central to exploring novel applications of TIs such as the formation of Majorana fermions in TI-

superconductor heterostructures [24], a viable new venue for realizing quantum computing, and dissipationless switching of magnetization in TI-ferromagnet hybrids [25], desirable for data-recording. Furthermore, because the formation of spirals creates spiral cores that are effectively bulk line defects, knowledge of the growth mechanism also allows the control of the density and types of spirals, necessary to investigate whether their cores do indeed support the topologically-protected 1D states, which would provide perfect bulk conducting channels and increase the figure of merit for thermal electrical applications [26].

In this Letter, we report the observation of spiral growth during MBE of Bi_2Se_3(111) on epitaxial graphene/SiC(0001) using *in situ* scanning tunneling microscopy (STM). We find that due to the weak interaction with the substrate, Bi_2Se_3 growth starts with the nucleation of two-dimensional islands, even with the presence of SiC steps. Contrary to dislocation-mediated spiral growth, we find that the Bi_2Se_3 spirals form as a result of the pinning of the 2D growth fronts by jagged step edges of the substrate or by domain boundaries formed during the coalescence of the 2D islands, both of which mimic the role of screw dislocations in the Burton, Carbrera, and Frank (BCF) model of spiral growth [19]. The winding of the as-created growth fronts around the pinning centers leads to the formation of spirals. As this model of spiral growth assumes only the pinning of 2D growth fronts at substrate steps or domain boundaries, conditions that are commonly met in the MBE growth of Bi_2Se_3 on single crystalline substrates [16-18] and hot-wall epitaxy of Bi_2Te_3 on Kapton and SiO_2 substrates [27], the mechanism should also be applicable to these cases. Finally, the growth of spirals provides an ideal platform to investigate the scattering of Bi_2Se_3(111) surface states off the spiral steps by STS, allowing us to experimentally demonstrate that the 1D helical mode associated with a line defect is indeed not supported by a strong TI like Bi_2Se_3 [5-7].

Experimental investigations were carried out on Bi_2Se_3 films grown on epitaxial graphene/SiC(0001) [28] at 275-325 ^oC. Bi and Se are supplied via either a single source of Bi_2Se_3 flakes in a p-BN crucible heated to 600 ^oC; or separate Knudsen cells heated to 460 and 250 ^oC, respectively. Electrochemically etched polycrystalline W tips, or mechanically sharpened Pt tips were used to take STM images at room temperature and 78 K. dI/dV spectra and images were taken using lock-in techniques.

Shown in Fig. 1(a) is an STM image of a Bi_2Se_3 film 30 QL thick, exhibiting predominately triangular spirals (density ~ $1.5x10^9/cm^2$) with type *B* edges, normal to [-211] or equivalent directions. A close-up view of a spiral is shown in Fig. 1(b), where the growth front winds around the core in the clockwise direction. In general, the spirals are characterized by atomically smooth terraces 10 to 100 nm in width, as determined from line profiles such as *AB* shown in Fig. 1(b). The step height is ~ 0.5 nm close to the core, and ~ 0.95 nm away from it, consistent with one Bi_2Se_3 QL. The atomic structure of the spiral core is shown in Fig. 1(c), where a step is created from the center to the lower left, clearly resembling a screw dislocation emerging at the surface [22]. The close-packed structure has a spacing of 4.1 Å, characteristic of the (1x1) periodicity of Bi_2Se_3(111). Note also that the spiral density decreases with increasing film thickness, which can be attributed to the coalescing and merging of spirals, similar to the spiral growth of GaN on SiC(0001) [22].

The structural properties of the Bi_2Se_3 films were characterized by x-ray diffraction and Raman spectroscopy. As shown in Fig. 1(d), only the (003) family diffraction peaks are observed, consistent with earlier studies of Bi_2Se_3 films grown on Si(111) and GaAs(111)B substrates [16,17]. The full width at half maximum of the θ-2θ rocking curve is found to be 0.2^o for a 30 QL film, indicating high film quality.

A typical Raman spectrum of the film is shown in Fig. 1(e). Two characteristic peaks at 129.5 and 171.7 cm^{-1} are observed, corresponding to the in-plane E_g^2 and out-of-plane A_{1g}^2 vibrational modes, respectively [29]. While the peak at lower frequency is shifted by (~+2 cm^{-1}) compared with that of a bulk Bi_2Se_3 crystal taken with the same spectrometer, there are little changes in the line shape of both peaks, further confirming excellent film quality.

These results, and others reported in earlier studies [16-18, 27], indicate that spiral growth is universal during vapor phase deposition of high quality Bi_2X_3 (X=Se, Te) films regardless of the substrate used. To address the origin of spiral formation, we examined the early stages of Bi_2Se_3 growth as shown in Fig. 2(a,b). Several observations are immediately evident. First, Bi_2Se_3 growth proceeds as 2D nucleation as opposed to step flow, even with the presence of a high density of SiC steps. Varying Bi/Se flux ratio and substrate temperature only changes island shape and size, and not the nature of 2D growth. Second, these Bi_2Se_3 islands are mostly triangular in shape with type *B* edges. Third, the growth downwards over a lower step seems unencumbered (Fig. 2(b)). Line profile *AB* clearly shows one QL Bi_2Se island rolling over a SiC bilayer step.

However, for growth upwards over an upper step, the situation is more complicated, depending on the relative angle between Bi_2Se_3 growth front and the SiC step, as well as the shape of the SiC step edge. An example is shown in Fig. 2(a) where a QL Bi_2Se_3 island, originated from a pit of the lower SiC terrace, climbs over a straight double SiC bilayer step, while maintaining relatively straight type *B* edges. An interesting case develops (Fig. 2(b)), however, when a Bi_2Se_3 island intercepts a jagged SiC step of the upper terrace, where two spirals, coiling in opposite directions, are formed with both of their cores being exactly at the step edge.

Additional spirals can also form at the intermediate stages of growth. Shown in Fig. 2(c) is an STM image of a film ~ 6 QLs thick, where eight spirals are present, most of which originated from domain boundaries resulting from coalescence of Bi_2Se_3 islands (one marked by an arrow). An atomic resolution image of one such boundary is shown in Fig. 2(d), where a 3^o angle is found between the two domains. These results clearly indicate that the spiral cores are not related to dislocations, but rather originate from SiC step edges and domain boundaries at the initial and intermediate stages of growth, respectively.

To further address the origin of spiral formation, we examine the stacking of Bi_2Se_3 along the [111] direction (Fig. 3(a)) by first-principle calculations using the Full-potential Linearized Augmented Plane Wave (FLAPW) method as implemented in flair [30], and the generalized gradient approximation (GGA), including full structural relaxations (lattice and internal parameters). Stretching the crystal along the c-axis by 20% (or even more) leaves the in-plane lattice parameter essentially unchanged, and the nearest neighbor bond lengths within the QL constant to within ~0.02 Å. In addition, the resulting distortion energy is quite small, ~15 meV/QL, confirming the weak bonding between the QLs. Such a unique structure clearly favors 2D growth, with the growth front determined by the Bi_2Se_3(111) steps: type *A* edge, normal to $[\bar{1}2\bar{1}]$ or equivalent directions, with two dangling bonds per edge atom; and type *B*, normal to $[\bar{2}11]$ or equivalent directions, with only one dangling bond per edge atom. With weak interactions with the graphene/SiC substrate to facilitate fast surface diffusion of Bi and Se adatoms to existing Bi_2Se_3 island edges, type *A* step will grow much faster, resulting in the near triangular Bi_2Se_3 islands/spirals with predominately type *B* steps (c.f., Fig. 2(a,b)). Furthermore, such a structure should also favor the unencumbered growth of TI islands over lower terraces.

For growth over an upper terrace, when a Bi_2Se_3 QL layer intercepts a single SiC step of 0.26 nm, it can be pinned initially. While the island continues to grow laterally around the pinning point on the lower terrace, new growth fronts are created that mirror the shape of the SiC step edge. As most existing 2D islands exhibit predominantly type *B* edges, this encounter can create type *A* edges with a much faster growth rate, i. e., opportunities that enable the Bi_2Se_3 island to make the "leap" to the upper terrace, even at an expense of ~20% stretching at the step edge. With a barrier of only ~15 meV for such stretching, the unique stability of Bi_2Se_3 along the [111] direction makes this energetically possible. In the case of a straight SiC step (c.f., Fig. 3(b)), only type *A* front is created, which would unilaterally extend over the upper terrace, and therefore no spiral is formed.

On the other hand, when the substrate step edge is jagged, more than one growth fronts can be created. An example is shown in Fig. 3(c), where an additional type *A* step is produced after the type *B* front is pinned. With its much faster growth rate, this step would "climb over" the upper terrace first, and resumes the preferred 2D growth on the upper terrace in all directions. When the new growth front encounters the original pinned step *B* (from the lower terrace), growth proceeds via a similar mechanism where pinning occurs initially which results in the creation of a second step *A* (parallel to the original step B, but in opposite direction), facilitating its further growth over the Bi_2Se_3 island. This clock-wise rotation leads to the formation of a spiral such as the one on the left in Fig. 2(b). Similarly, a counter clockwise spiral is formed with an inversely shaped SiC step. In both cases, the cores are vertically displaced by the height of the pinning SiC step at the jagged point, and the step height is one QL away from it, resembling that of a screw dislocation emerging at the surface [22, 27]. Note that this model also applies to the case when the growth fronts are pinned instead at domain boundaries where two Bi_2Se_3 islands

of different heights merge. In both cases, the pinning of growth fronts at geometrical constrains mimics the role of screw dislocations in the BCF theory of spiral growth [19].

The model also assumes that the pinning SiC steps is less than one QL in height, which is satisfied since the steps on 6H-SiC(0001) are mostly single-, double-, and triple-layer heights of 0.26 nm, 0.52 nm, and 0.78 nm, respectively. In the case of higher than triple-layer steps such as those often found on vicinal substrates [31], the energy barrier to distort the Bi_2Se_3 QL to grow over them will be significantly higher, leading to reduced pinning centers at step edges at the early stages of growth. While spirals can still form from the domain boundaries, the overall spiral density will be significantly reduced. Our growth of Bi_2Se_3 on vicinal SiC substrates with a 3.5^o miscut has indeed led to a lower spiral density.

Overall, this new spiral growth mechanism assumes only the pinning of 2D growth fronts at substrate steps or domain boundaries, conditions that are common in the MBE growth of Bi_2Se_3 on single crystal substrates [16-18], and in the hot-wall epitaxy of Bi_2Te_3 on Kapton and SiO_2 substrates [27]. Therefore, we expect that the model should also be applicable to these cases and, more generally, to the epitaxial growth of other van der Waals materials on weakly interacting substrates.

This spiral growth of Bi_2Se_3 provides an ideal platform to investigate the scattering of its surface states off spiral steps using tunneling spectroscopy. Shown in Fig. 4(a) is a dI/dV spectrum taken on the Bi_2Se_3(111) surface, exhibiting a general V-shape with the Dirac point (E_D) at 240 meV below the Fermi level, consistent with earlier studies [11, 14, 15]. Shown in Fig. 4(b) and (c) are STM and dI/dV images taken simultaneously over a regular array of parallel steps and three spiral cores. Close inspection of the images reveals that while the local densities of states are greatly enhanced near steps, no discernable augmentation is evident at the spiral

cores in the range of energies studied (150-375 meV below E_F) (Fig. 4(d)). This confirms that the 1D helical mode of line defects is not allowed for a strong TI like Bi_2Se_3 [5-7].

Additional near periodic patterns are, however, clearly evident near the step edges in the dI/dV images, which are likely standing waves caused by the scattering of the Bi_2Se_3 surface states off the step edges [12, 13], similar to that observed on metal surfaces [32]. Nevertheless, three factors needed to be considered in any future modeling of standing waves on TI surfaces: 1) the transmission of electrons through TI steps [33]; 2) faster decay of wave amplitude from the step edge due to the suppression of back scattering [34]; and 3) the contribution of the 2D electron gas near the TI surface due to band bending [35].

In summary, we observed spirals during the MBE growth of Bi_2Se_2 on epitaxial graphene/SiC(0001), which is explained by a non-dislocation-mediated spiral growth mechanism that should also apply to the epitaxy of other van der Waals materials on weakly interacting substrates. We have also directly imaged the standing waves caused by scattering of the Bi_2Se_3 surface states off the spiral steps and cores, and confirmed that the 1D helical mode of a line defect is not supported by strong TIs such as Bi_2Se_3.

Acknowledgement: Funding for this work is provided by NSF (DMR-0706359) and DMR-1105839).

Figure captions:

Fig. 1 (a) STM image of a 30 QL Bi_2Se_3 film grown on epitaxial graphene/SiC taken at room temperature, showing the formation of spirals (I_t=0.79 nA, V_s=-0.047 V). (b) Close-up view of a spiral, and line profile across *AB* (I_t=1.17 nA, V_s=-1.70 V). (c) Atomic resolution image of the spiral core taken at 78 K, showing a step originated from the spiral core in the center of the image (I_t=1.30 nA, V_s=1.10 V). (d) X-ray diffraction of a 30 QL Bi_2Se_3 film using Cu $K_{\alpha 1}$ emission, with the high intensity SiC peak removed. Additional small peaks are due to additional diffractions from extraneous x-ray emissions of the Cu source, e.g., the peak at 17.41° is a side peak of (006) due to Cu $K_{\beta 1}$ (λ=0.1392 nm). Inset: θ-2θ rocking curve. (e) Raman spectra of a 30 QL Bi_2Se_3 film, showing two characteristic peaks at 129.5 and 171.7 cm^{-1}.

Fig.2 (a) STM image of a Bi_2Se_3 island 2 QLs high with the arrow marking a SiC step (I_t=0.10 nA, V_s=-0.48 V). (b) STM image of two spirals originating at a SiC step edge (I_t=0.28 nA, V_s=-0.27 V), with line profile *AB* crossing a 1 QL Bi_2Se_3 island overlaid on top of a double bilayer SiC step. (c) STM image of a 6 QL Bi_2Se_3 film at the intermediate stages of spiral growth (I_t=0.10 nA, V_s=-0.70 V). Images shown in (a-c) are taken at room temperature. (d) Atomic resolution image taken at 78 K, showing the atomic structure of a grain boundary on Bi_2Se_3(111) observed on the 6 QL film (I_t=1.10 nA, V_s=0.30 V). The two straight lines indicate the 3° angle between the two neighboring domains.

Fig. 3 (a) Ball-and-stick models of Bi_2Se_3 along the [111] direction, and a 2D island with type *A* [$\bar{1}$ 12 $\bar{1}$] steps with two dangling bonds per edge atom and type *B* [$\bar{2}$ 11] steps with one dangling

bond. (b) Schematic diagrams showing a Bi_2Se_3 island leaping over a straight upper SiC step. (c) Schematic diagrams (side and top views) illustrating the formation a clock-wise spiral.

Fig. 4 (a) dI/dV spectrum taken on the Bi_2Se_3(111) surface at 78 K with the Dirac point marked. (b) STM image and (c) dI/dV map of the same area obtained simultaneously at 78 K, with three spiral cores labeled *1-3* (I_t=0.50 nA, V_s=-0.15 V). (d) Energy-dependent dI/dV images of the boxed area in (c).

References:

1. H. Zhang, C. -X. Liu, X. -L. Qi, X. Dai, Z. Fang, S. -C. Zhang, Nature Phys. **5**, 438 (2009).
2. R. Venkatasubramanian, E. Siivola, T. Colpitts, and B. O'Quinn, Nature **413**, 597 (2001).
3. D. Teweldebrhan, V. Goyal, M. Rahman, and A. A. Balandin, Appl. Phys. Lett. **96**, 053107 (2010).
4. L. Fu, C. L. Kane, and E. J. Mele, Phys. Rev. Lett. **98**, 106803 (2007).
5. Y. Ran, Y. Zhang, A. Vishwanath, Nature Phys. **5**, 298 (2009).
6. J. C. Y. Teo and C.L. Kane, Phys. Rev. B **82**, 115120 (2010).
7. K. -I. Imura, Y. Takane, and A. Tanaka, Phys. Rev. B **84**, 035443 (2011).
8. D. Hsieh et al., Nature **460**, 1101 (2009).
9. Y. L, Chen et al., Science **325**, 178 (2009).
10. Y. Zhang et al., Nature Phys. **6**, 584 (2010).
11. Y. S. Hor et al., Phys. Rev. B **79**, 195208 (2009).
12. T. Zhang et al., Phys. Rev. Lett. **103**, 266803 (2009).
13. Z. Alpichshev, Phys. Rev. Lett. **104**, 016401 (2010).
14. P. Chen et al., Phys. Rev. Lett. **105**, 076801 (2010).
15. S. Kim et al., Phys. Rev. Lett. **107**, 056803 (2011).
16. H. D. Li et al., N. J. Phys. **12**, 103038 (2010).
17. A. Richardella et al., Appl. Phys. Lett. **97**, 262104 (2010).
18. J. Chen et al., Phys. Rev. Lett. **105**, 176602 (2010).
19. W. K. Burton, N. Cabrera, and F. C. Frank, Philos. Trans. R. Soc. London **243**, 299 (1951).
20. A. Karma and M. Plapp, Phys. Rev. Lett. **81**, 4444 (1998).

21. B. Heying, E. J. Tarsa, C. R. Elsass, P. Fini, S. P. DenBeaars, and J. S. Speck, J. Appl. Phys. **85**, 6470 (1999).

22. Y. Cui and L. Li, Phys. Rev. B **66**, 155330 (2002).

23. T. Akasaka, Y. Kobayashi, and M. Kasu, Appl. Phys. Lett. **97**, 141902 (2010).

24. L. Fu and C. L. Kane, Phys. Rev. Lett. **100**, 096407 (2008).

25. I. Garate and M. Franz, Phys. Rev. Lett. **104**, 146802 (2010).

26. O. A. Tretiakov, Ar. Abanov, S. Murakami, and J. Sinova, Appl. Phys. Lett. **97**, 073108 (2010). O. A. Tretiakov, Ar. Abanov, and J. Sinova, Appl. Phys. Lett. **99**, 113110 (2011).

27. M. Ferhat, J. C. Tedenac, and J. Nagao, J. Cryst. Growth **218**, 250 (2000).

28. Y. Qi, S. H. Rhim, G. F. Sun, M. Weinert, and L. Li, Phys. Rev. Lett. **105**, 085502 (2010).

29. W. Dang, H. Peng, H. Li, P. Wang, and Z. Liu, Nano Lett. **10**, 2870 (2010).

30. M. Weinert, G. Schneider, R. Podloucky, and J. Redinger, J. Phys. Condens. Matter **21**, 084201 (2009).

31. H. Nakagawa, S. Tanaka, and I. Suemune, Phys. Rev. Lett. **91**, 226107 (2003).

32. M. F. Crommie, C. P. Lutz, and D. M. Elgler, Nature **363**, 524 (1993).

33. J. Seo, P. Roushan, H. Beidenkopf, Y. S. Hor, R. J. Cava, A. Yazdani, Nature **466**, 343 (2010).

34. R. R. Biswas and A. V. Balatsky, Phys. Rev. B **83**, 075439 (2011).

35. B. Marco et al., Nature Comm. **1**, 128 (2010).

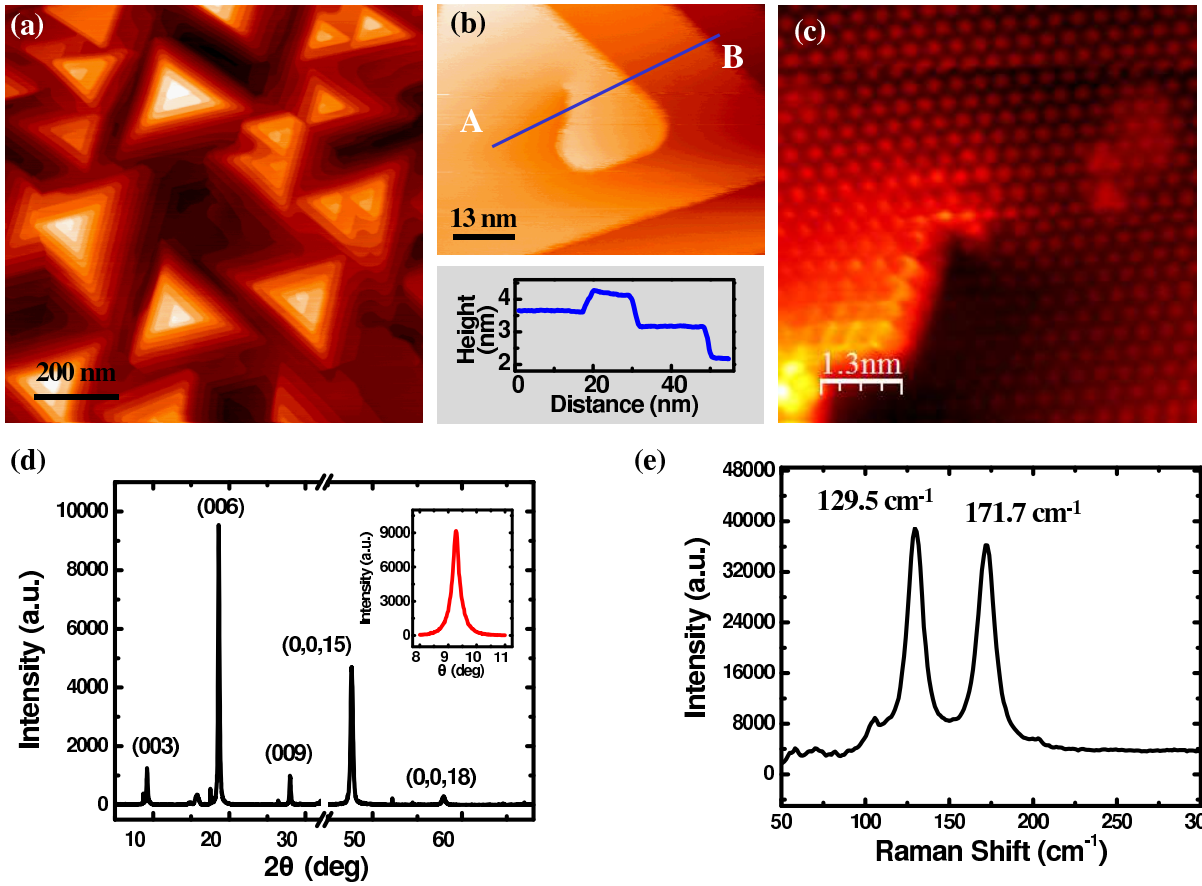

Figure 1 LK12946 05DEC2011

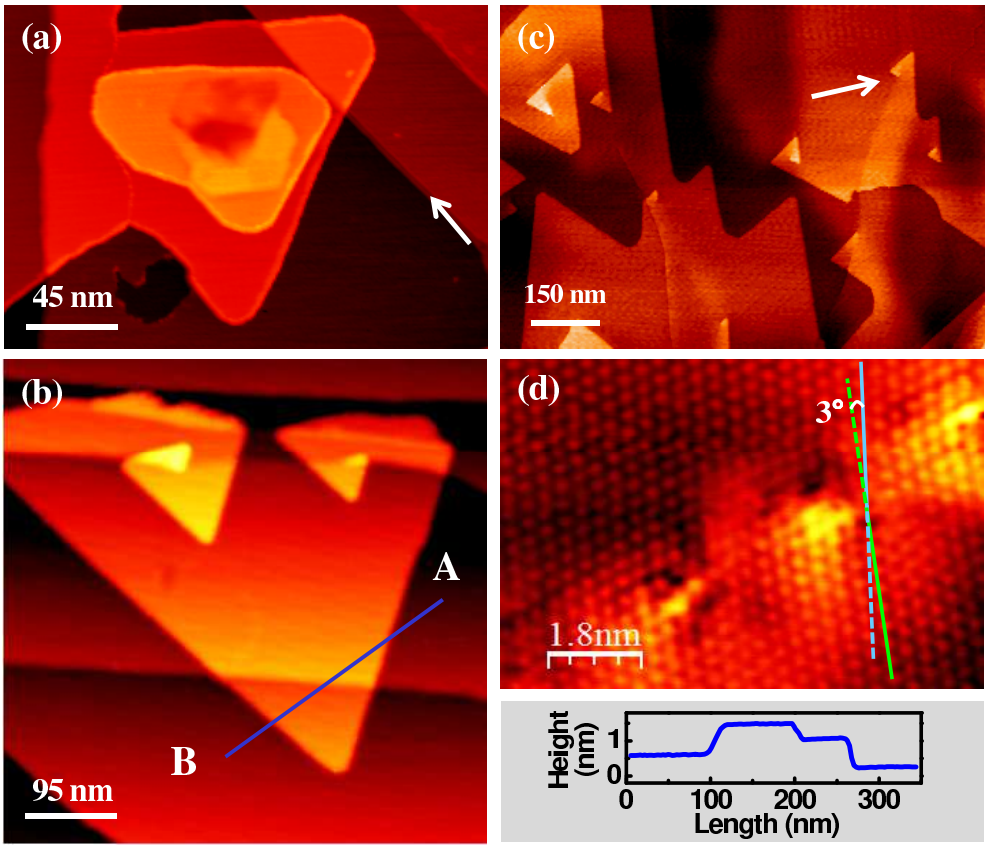

Figure 2 LK12946 05DEC2011

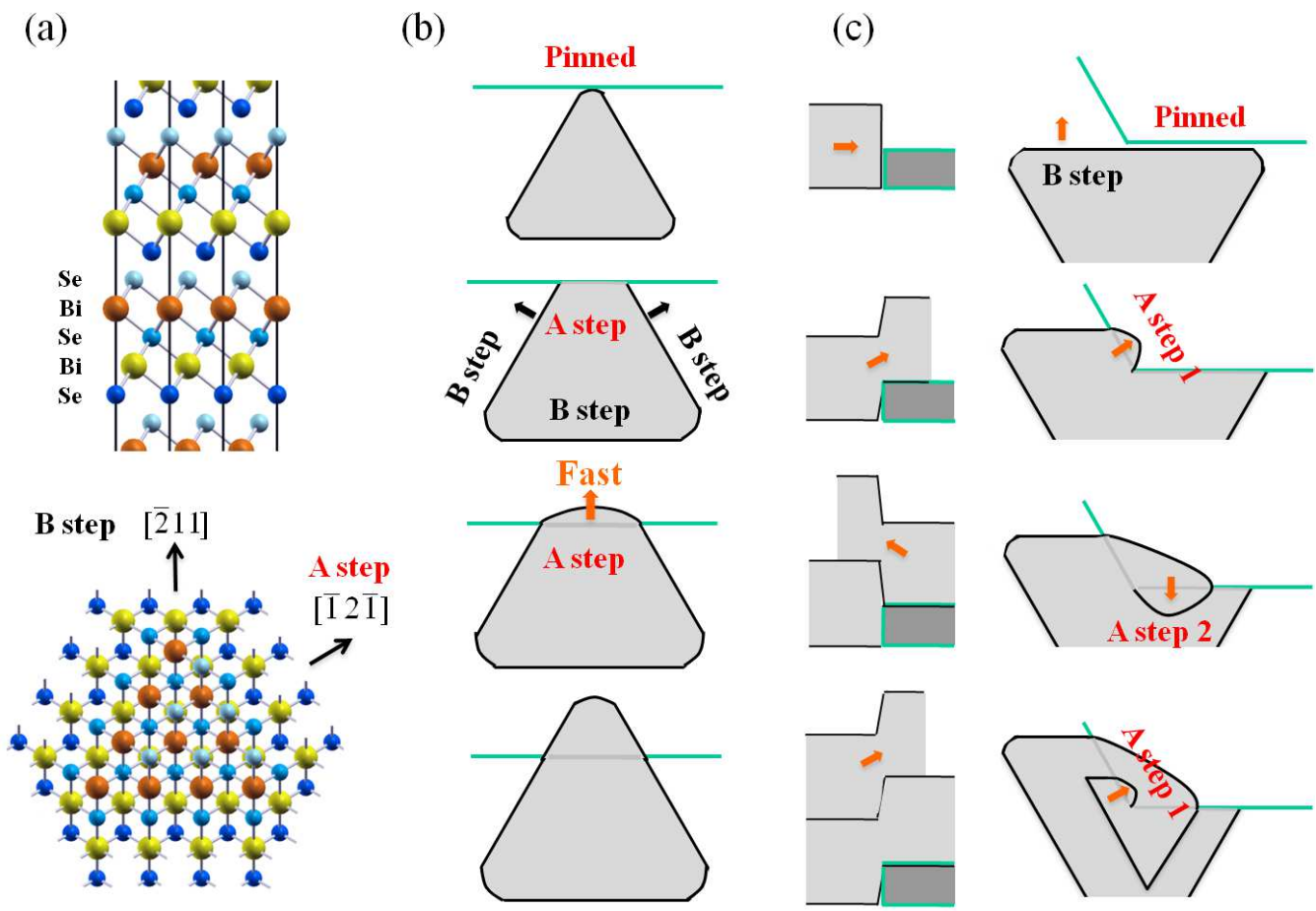

Figure 3 LK12946 05DEC2011

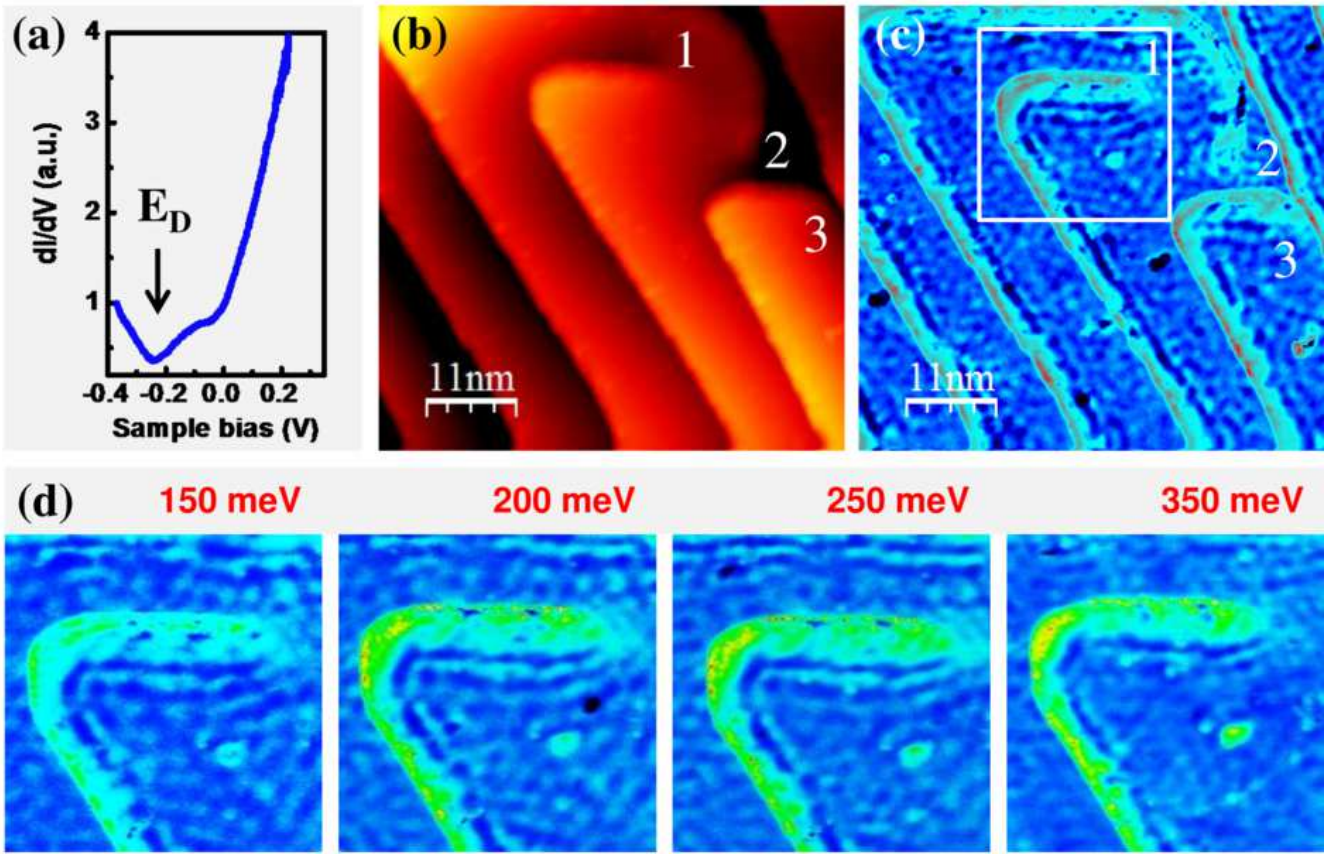

Figure 4 LK12946 05DEC2011